MOLECULAR PHYSICS 2679582
https://doi.org/10.1080/00268976.2026.2679582

Taylor & Francis
by informa

SPECIAL ISSUE IN HONOUR OF FRÉDÉRIC MERKT

Photoabsorption and photoionization of N_2 near the first ionisation threshold

Ananya Sen[a]*, Nelson de Oliveira[b], Ugo Jacovella [c], Bérenger Gans[c], Séverine Boyé-Péronne[c], David M. P. Holland[d], Wim Ubachs [e], Alan Heays[f]**, Stephen T. Pratt[a] and Christian Jungen[g]

[a]Chemical Sciences and Engineering Division, Argonne National Laboratory, Argonne, IL, USA; [b]Synchrotron SOLEIL, Saint-Aubin, Gif-sur-Yvette, France; [c]Institut des Sciences Moléculaires d'Orsay, CNRS, Université Paris-Saclay, Orsay, France; [d]STFC Daresbury Laboratory, Warrington, UK; [e]Department of Physics and Astronomy, Vrije Universiteit Amsterdam, Amsterdam, The Netherlands; [f]J. Heyrovsky Institute of Physical Chemistry, Czech Academy of Sciences, Prague 8, Czech Republic; [g]Laboratoire Aimé Cotton du CNRS, Université de Paris-Saclay, Orsay, France

ABSTRACT

The photoabsorption and photoionization spectra of molecular nitrogen, N_2, near the first ionisation threshold display numerous intense resonances that have not been satisfactorily assigned to date. Principal among these is a pair of broad resonances between 126,200 and 126,600 cm^{-1} commonly referred to as the "cathedral" bands. Here, we present new double-resonance photoionization spectra in this region recorded via the $a''\ ^1\Sigma_g^+, v' = 0$ intermediate state as well as new high-resolution, vacuum-ultraviolet photoabsorption spectra of $^{14}N_2$,$^{14}N^{15}N$, and $^{15}N_2$ to provide additional insight into the assignment of these features. Progress towards a fully consistent interpretation of the existing data on these bands is discussed, and a route towards a comprehensive description of the N_2 absorption spectrum up to the $B\ ^2\Sigma_u^+$ state of N_2^+ is proposed.

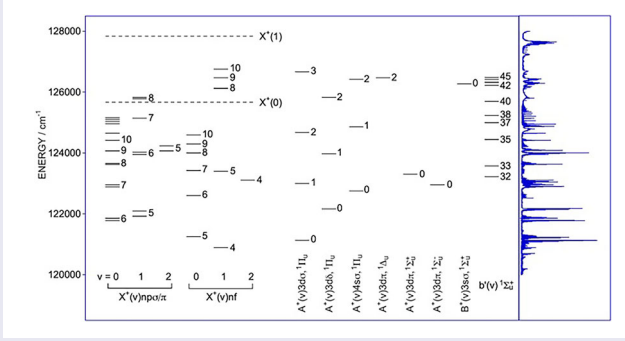

ARTICLE HISTORY
Received 13 March 2026
Accepted 8 May 2026

KEYWORDS
Vacuum ultraviolet Fourier transform spectroscopy; double-resonance spectroscopy; photoionization; Rydberg states

1. Introduction

Rovibronic interactions strongly influence a wide range of excited state dynamics and chemistry [1,2]. Over the years, considerable theoretical progress has been made that allows the calculation and modelling of many excited states and their interactions, providing confidence in our understanding and methodologies [2]. It is therefore sobering to realise that despite many decades of study [3–20], a comprehensive and consistent assignment of the near-threshold photoabsorption and photoionization spectra of molecular nitrogen, N_2, does not yet exist [21–37]. In particular, the origin of many significant features in these spectra is only tentatively understood. While this situation may seem surprising for a molecule as fundamental and simple as N_2, the complexity arises through the interactions among a substantial number of Rydberg series converging to rovibrational levels of the $X\ ^2\Sigma_g^+$, $A\ ^2\Pi_u$, and $B\ ^2\Sigma_u^+$ states of N_2^+, as well as high vibrational levels of the $b'\ ^1\Sigma_u^+$ valence state. The complexity is further enhanced by singlet-triplet interactions [38–41].

The current understanding of the photoabsorption spectrum of N_2 up to the ionisation threshold (viz. 125,667.028 ± 0.015 cm^{-1} [42]) has been developed

CONTACT Christian Jungen christian.jungen@universite-paris-saclay.fr, christian.jungen@orange.fr Laboratoire Aimé Cotton du CNRS, Université de Paris-Saclay, Bâtiment 505, Orsay91405, France
*Present address: Schrodinger Inc., 13th Floor, Unit 1, Orwell Block, Salarpuria Sattva Knowledge City, Silpa Gram Craft Village, Madhapur, Hyderabad, Telangana 500081, India
**Present address: Manaaki Whenua Landcare Research, Bioeconomy Science Institute, PO Box 69040, Lincoln 7640, New Zealand

over many years [6]. Below $\sim$105,000 cm^{-1}, the photoabsorption spectrum is dominated by transitions to Rydberg series converging to the N_2^+ X^+ $^2\Sigma_g^+$ $v^+ = 0 - 2$ levels, and to a long vibrational progression of the b' $^1\Sigma_u^+$ and b $^1\Pi_u$ valence states [4–10]. Strong interactions between the Rydberg and valence states result in substantial perturbations and irregularities in the spectrum. Levels above the adiabatic dissociation threshold (78691.09 $\pm$ 0.15 cm^{-1}) [43] are also subject to predissociation [11,12]. Insight from Dressler [7] and Lefebvre-Brion [8] provided the foundation for the analysis of the long vibrational progressions of the valence states. While the $A^+(0)3s\sigma_g$ (o $^1\Pi_u$, $v = 0$) level at 105,710 cm^{-1} is the first one-photon excitation allowed Rydberg state based on the N_2^+ A $^2\Pi_u$ state, at higher energies transitions to the $A^+(v^+)4s\sigma_g$, $A^+(v^+)3d\sigma_g$, $A^+(v^+)3d\pi_g$, and $A^+(v^+)3d\delta_g$, Rydberg configurations become accessible with one-photon excitation, adding complexity to the spectrum. (Here we use the previously defined notation to define the Rydberg configuration, with $A^+(v^+)$ denoting the electronic and vibrational level of the ion core and $n\ell\lambda_g$ providing the symmetry of the Rydberg electron.) In a series of papers, Huber, Jungen, and collaborators [17–20], performed a detailed analysis of the jet-cooled absorption spectrum up to $\sim$ 125, 000 cm^{-1}. The jet cooling provided substantial simplification of the spectrum but retained sufficient rotational structure to aid the analysis. Using multichannel quantum defect theory, MQDT, to account for the multiple interacting states [17–19], they provided an essentially complete account of the spectrum, although the assignment of a few features remained ambiguous [20].

At higher energies, the first $B^+(v^+)n\ell\lambda_g$ Rydberg configurations become accessible. Here, the additional interactions, as well as the interplay between autoionisation and predissociation, make the region between the X^+ $^2\Sigma_g^+, v^+ = 0$ and A^+ $^2\Pi_u$, $v^+ = 0$ thresholds a region of maximum complexity. Above the A^+ $^2\Pi_u$, $v^+ = 0$ threshold at 134,683.9 cm^{-1}, the spectra become simpler again with the very regular pattern of the three Rydberg series converging to the B^+ $^2\Sigma_u^+$, $v^+ = 0$ threshold [14,37].

One notable region within the zone of maximum complexity lies between 126,200 cm^{-1} and 126,600 cm^{-1}. Here, there are multiple bands displaying a large range of linewidths and intensities, with the two dominant features having the appearance of the two towers of a cathedral [21,25,28–31]. Experimental attempts to unravel this structure have included high-resolution, vacuum-ultraviolet photoabsorption and photoionization spectra from 10 K to room temperature [17,28,31,36], hot-band studies using a microwave discharge [21], isotopic studies using $^{14}N_2$, $^{14}N^{15}N$, and $^{15}N_2$ [31,35], photoelectron angular distribution measurements [36], and double-resonance ionisation experiments via the a $^1\Pi_g, v = 5$ vibronic state [25]. At the same time, theoretical attempts have involved *ab initio* quantum chemistry, theoretical spectroscopy, and analysis using MQDT [29,30].

Figure 1 shows a small section ($\sim$1200 cm^{-1}) of the VUV Fourier transform (FT) photoabsorption spectrum of N_2 at three different temperatures just above the ionisation threshold (this work, see below). Figure 2 shows a schematic vibronic energy level diagram for N_2 over a far larger energy range ($\sim$1 eV) that puts the details of the 'tower region' into a larger perspective. At the right of the Figure, the VUV-FT spectrum from the SOLEIL synchrotron [44–46] is drawn to scale. It may be seen that the strong absorptions in the N_2 VUV absorption spectrum up to the IP are dominated by absorption to the $A^+(v^+)n\ell\lambda$ Rydberg configurations. The assignments of the bands come from a number of different sources [17–20,25,26,28–31], most of which are reasonably secure. The first cathedral tower has been assigned [25] to the lowest singlet Rydberg state associated with the B^+ $^2\Sigma_u^+$ core, namely $B^+(0)3s\sigma_g$, $^1\Sigma_u^+$. The assignment of the second tower at $\sim$126,420 cm^{-1}, however, is still the subject of considerable disagreement, even with respect to its assignment as a Σ or Π state. In particular, McCormack *et al.* [25] and Lefebvre-Brion [29,30] have assigned this feature as the $A^+(2)4s\sigma$, $^1\Pi_u$ and $A^+(2)3d\sigma$, $^1\Pi_u$ state, respectively, while Sommavilla and Merkt have reported simulations of their jet-cooled absorption and ionisation spectra that suggest the state has Σ symmetry [31]. In their double-resonance experiments, McCormack *et al.* [25] did not actually observe the feature at 126,420 cm^{-1}, and made their assignment based on the process of elimination and the positions of lower energy states. Their assignment as a $v = 2$ band is supported by the isotopic studies of Randazzo *et al.* [35]. Lefebvre-Brion [29,30] based her assignments on theoretical considerations and earlier spectroscopic studies. Sommavilla and Merkt [31] actually identified two bands contributing to the feature at 126,420 cm^{-1}. However, the simplification provided by the jet-cooled spectra limited the rotational structure of the bands to $J'' <\sim 3$, and thus the extent of their analysis.

Here we report new double-resonance spectra of $^{14}N_2$ that use the $X^+(0)$ $3s\sigma_g, a''$ $^1\Sigma_g^+$ intermediate state to access the ungerade manifold in the threshold region. These spectra were recorded for a broad range of intermediate rotational levels to map out the rotational structure of the upper states.

We also present new high-resolution, room-temperature photoabsorption data for $^{14}N^{15}N$, and $^{15}N_2$ from the vacuum-ultraviolet Fourier transform spectrometer at the SOLEIL Synchrotron [44–46], as well as analogous

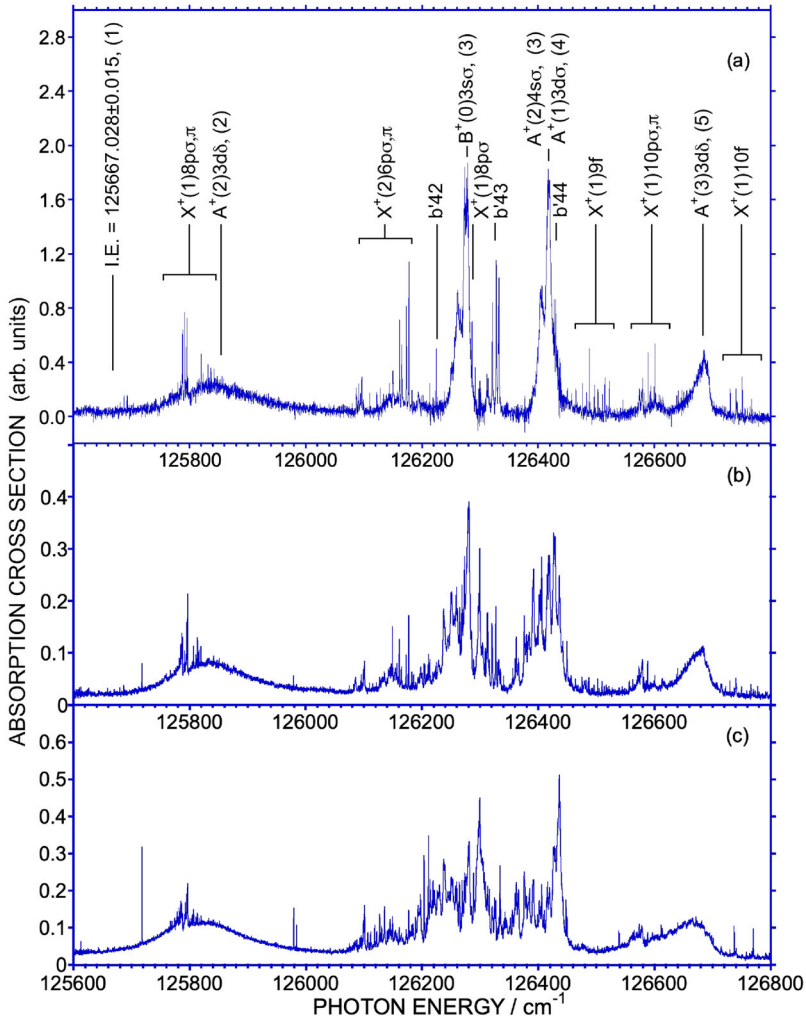

Figure 1. The high-resolution photoabsorption spectrum of $^{14}N_2$ between 125,600 and 126,800 cm^{-1} (this work). (a) Supersonic jet ~ 18 K, (b) 77 K, (c) 298 K. Assignments for labelled peaks are from: (1) Ref. [42], (2) Ref. [18] (3) Ref. [25], (4) Ref. [29], (5) Ref. [26].

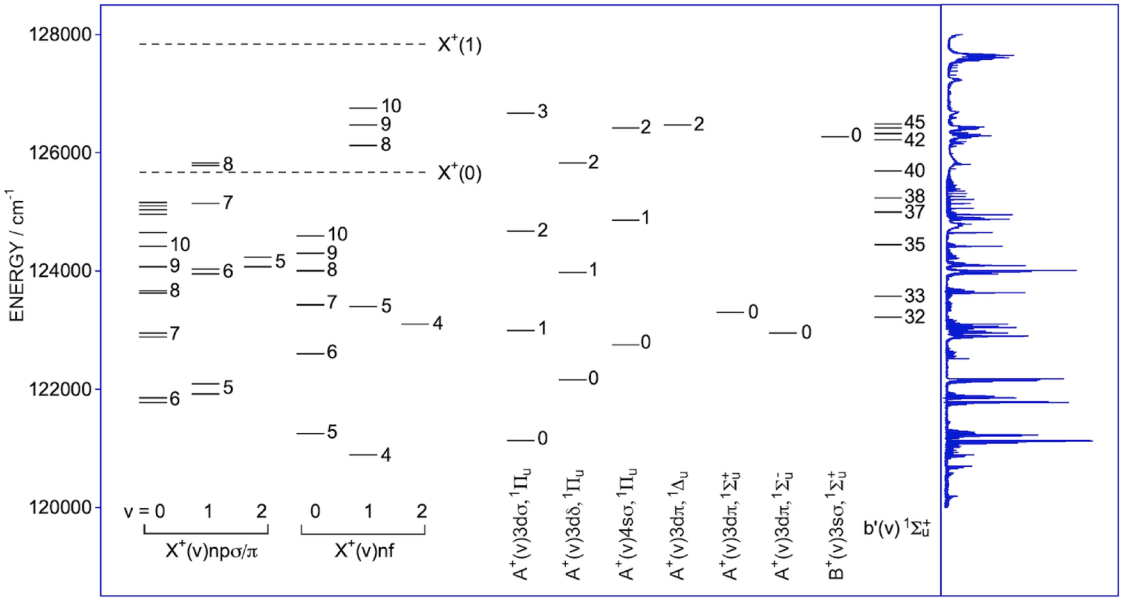

Figure 2. Schematic energy level diagram using some of the energies and assignments from Ref. [18].

data for $^{14}N_2$ and $^{15}N_2$ in a cooled cell at 77 K, and for $^{14}N_2$ in a supersonically cooled molecular beam at ~18 K. The absorption spectra extend across a broad range of nearly 5 eV of the nitrogen spectrum, from ~114,100 cm^{-1}, well below the first ionisation threshold, to 153,000 cm^{-1}, just above the $B^+\,^2\Sigma_u^+, v^+ = 0$ threshold.

Even with the new double-resonance and absorption data, it will be clear from the discussion that there are still a number of seemingly contradictory observations and unresolved questions. We believe a more global analysis of the spectra is necessary to resolve these issues, and that the comprehensive absorption spectra presented here will ultimately allow such an analysis. In particular, we have initiated an effort to extend the multichannel quantum defect theory (MQDT) analysis of Refs. [17–19], which was largely confined to the region below the ionisation threshold, to the higher energies of the present study. The initial stages of that effort are also described here.

2. Experimental and theoretical considerations

2.1. Double-resonance experiments

As described previously, the experiments were performed by using a differentially pumped mass spectrometer [47,48]. The $^{14}N_2$ sample was introduced into the source chamber through a pulsed valve, and the resulting beam passed through a 1 mm skimmer into the interaction chamber. The molecular beam was crossed by two laser beams in the interaction region, resulting in N_2^+ ions that were detected by time-of-flight mass spectrometry. There was a constant DC field in the interaction region of ~ 75–125 V/cm^{-1}. The resonances of interest here have quite low n (typically 3-5), and this field is not expected to modify the spectra significantly.

Light for the two-photon $a''\,^1\Sigma_g^+, v = 0 \leftarrow X\,^1\Sigma_g^+, v'' = 0$ transition was generated by frequency tripling the output of a commercial Nd:YAG-pumped dye laser operating at about 607 nm, with a bandwidth at 202.3 nm of ~0.3 cm^{-1}. The wavelength was calibrated by using a commercial wavemeter. The probe beam was generated by frequency doubling the output of a second Nd:YAG-pumped dye laser, resulting in a bandwidth of the ultraviolet probe light of ~0.2 cm^{-1}. The uncertainty in the overall transition energies is estimated to be ±1 cm^{-1}. The two beams were combined by using a dichroic mirror and the collinear beams were focussed into the interaction region. The pulse energies of the pump and probe beams were ~10–20 μJ and 100–200 μJ, but because the two beams were focussed through a fused silica lens, the spot sizes differ in the interaction region, making it difficult to assess the relevant intensity of the two beams. The linear polarizations of both the pump and probe laser beams were parallel to each other and to the face of the imaging detector. The probe beam was typically delayed by ~100–200 ns from the pump beam to allow the separation of the signal generated by the pump beam alone, but varying the delay had little effect on the signal.

In the present experiment, the pump laser was used to excite the two-photon $a''\,^1\Sigma_g^+, v = 0, J \leftarrow X\,^1\Sigma_g^+, v'' = 0, J''$ transition, which has been characterised previously [49–51]. Here the initial state quantum numbers are labelled with a double prime, the intermediate $a''\,^1\Sigma_g^+$ state values with no prime, and the upper levels of the probe transitions by a single prime. The dominant feature of this two-photon band is a strong Q branch that creates a bandhead at low J''. This bandhead is not resolved in the present study. Specifically, two-photon $Q(J'')$ pump transitions with $J'' \leq 4$ are overlapped, and the corresponding double-resonance spectra include transitions from two or more intermediate levels. For higher J'' values, the pump transitions are well resolved. The pulsed valve creates a low rotational temperature in the molecular beam; thus, the valve was replaced by an effusive source, and the molecular beam skimmer was removed to record the spectra for high J'' levels.

The probe laser was used to excite the single-photon transitions from the $a''\,^1\Sigma_g^+, v = 0, J$ level into the spectral region of interest. Spectra were recorded by pumping the $Q(J'')$ branch transitions for $J'' = 0 - 14$. Since the ^{14}N atom has nuclear spin, $I = 1$, the resulting bands will have an intensity alteration of 2:1 with respect to even:odd rotational levels excited by the pump laser [52]. For ^{15}N, the nuclear spin is $I = 1/2$, and the intensity alteration is 1:3 with respect to even and odd rotational levels of the ground state.

2.2. Vacuum-ultraviolet Fourier transform spectroscopy

The Fourier Transform Spectrometer (FTS) on the DESIRS undulator beamline of the Synchrotron SOLEIL has been described in detail previously, de Oliveira *et al.* [44–46] and here we describe only those aspects that are relevant to the present measurements.

The spectra of $^{14}N_2$ were recorded using two different experimental configurations: (1) a 100 mm windowless flowing cell used to record high-resolution, room-temperature and liquid-nitrogen-cooled (77 K) spectra; and (2) a supersonic molecular beam produced using a slit-jet expansion. The slit size is $5 \times 1000\ \mu m^2$ and the photon beam propagates along the long axis of the slit to provide a cold, collision-free and field-free environment. The method to record and calibrate absolute absorption cross sections in the flowing cell has also been described previously [46]. For the present experiments, neat $^{14}N_2$

was used directly from the cylinder for all of the measurements. For $^{14}N^{15}N$, spectra were only recorded using the flowing cell at room temperature, while for $^{15}N_2$ liquid-nitrogen-cooled (77 K) spectra were also taken.

The free molecular jet set-up chamber is pumped by a 500 liters/s turbo pump and isolated from the main gas sample chamber by two 20 mm long tubes to provide an extra stage of differential pumping to the system. The jet-cooled spectra were recorded with stagnation pressures of 2 and 4 bar. Because the relative contribution of absorption by the molecular beam and the background gas is difficult to characterise, the absorption cross sections of the jet spectra are reported in arbitrary units, rather than as absolute cross sections. The spectrometer used the entire bandwidth of the undulator after the synchrotron light had passed through a harmonic-removing gas filter. The region of interest for the present study was fully covered by using the continuum of light from a single undulator setting. The resolution of ~ 0.33 cm^{-1} is confirmed from the narrowest lines in the spectrum.

2.3. MQDT analysis

In Refs. [17–19] multichannel quantum defect theory (MQDT) has been used to interpret the various Rydberg series and their mutual interactions. The analysis of Ref. [19] included rotational, vibrational and electronic channel couplings that correspond, in terms of the associated ionisation processes, to rotational, vibrational and electronic autoionisation. The theoretical approach of Ref. [19] thus involved Rydberg electrons with $\ell = 0 - 3$, as well as the two electronic core states $X^+\ ^2\Sigma_g^+$ (Rydberg electron with odd ℓ values) and $A^+\ ^2\Pi_u$ (Rydberg electron with even ℓ values). The channel couplings were described in terms of the frame transformation theory [53–55]. The parameters involved in the MQDT analysis of the near-threshold absorption spectrum, 42 quantum defects and 7 dipole transition moments, were determined purely empirically based on 597 observed rovibronic levels and 22 oscillator strength values of the N_2 absorption spectrum.

The analysis presented in Ref. [19] has perhaps been one of the most extensive applications of this theory to any molecule to date. However, spin effects were not considered at the time, and interactions of the Rydberg rovibronic levels with valence states were also not included, as well as Rydberg channels built on the $B^+\ ^2\Sigma_u^+$ core excited state. Also, in that earlier work decay processes such as predissociation or autoionisation were not considered. Nevertheless, a logical initial step in order to apply the MQDT approach to the new synchrotron VUV Fourier Transform spectra, and eventually to extend this analysis to higher excitation, consists in using the quantum defect parameters determined in Ref. [19] within the same theoretical framework as previously.

3. Results: experiments

3.1. Double-resonance spectra of $^{14}N_2$

We have recorded double-resonance spectra by pumping the rotationally resolved, two-photon $Q(J'')$ transitions in the $a''\ ^1\Sigma_g^+, v = 0 \leftarrow X\ ^1\Sigma_g^+, v'' = 0$ band, and probing in the region corresponding to a total energy of 126,250 cm^{-1} to 126,750 cm^{-1} relative to the $X\ ^1\Sigma_g^+, v'' = 0, J'' = 0$ level. While transitions to high Rydberg states that are described by Hund's case d or e may not show both P and R branches for each transition, the Rydberg states in the present energy range with $A^+\ ^2\Pi_u$ or $B^+\ ^2\Sigma_u^+$ cores have low principal quantum numbers and can be described by Hund's case a. As a result, both P and R branches are expected for $^1\Sigma_g^+ \rightarrow {}^1\Sigma_u^+$ transitions (including those to the $b'\ ^1\Sigma_u^+, v$ valence levels of vibrational quantum number, v, notated here as $b'v$), and P, Q, and R branches are expected for $^1\Sigma_g^+ \rightarrow {}^1\Pi_u$ transitions. In the latter case, the P and R branches access the $^1\Pi_u^+$ component of the upper state, and the Q branch accesses the $^1\Pi_u^-$ component. Comparing probe spectra for the $Q(J-1)$ and $Q(J+1)$ pump transitions to the $a''\ ^1\Sigma_g^+$ state allows the identification of $R(J-1)$ and $P(J+1)$ probe transitions to a common $^1\Sigma_u^+$ or $^1\Pi_u^+$ upper state with total angular momentum J. Probe transitions that do not appear for both the $Q(J-1)$ and $Q(J+1)$ pump transitions likely correspond to a Q-branch.

Figure 3 shows four representative double-resonance spectra in which rotational transitions have been determined through this process. Bands with unambiguous vibronic assignments are labelled accordingly. Perhaps the most striking observation in Figure 3 is the lack of evidence for any Q branches, which are expected for transitions from the $a''\ ^1\Sigma_g^+, v = 0$ level to low-principal quantum number $A^+(v^+)n\ell\lambda_g\ ^1\Pi_u$ and $B^+(v^+)nd\pi_g\ ^1\Pi_u$ levels. Specifically, there does not appear to be any evidence for a Q branch between the P and R transitions for the upper tower of the cathedral bands. Thus, the spectra confirm the earlier conclusion of Sommavilla and Merkt [31] that the state responsible for the upper tower behaves as a $^1\Sigma_u^+$ Rydberg state, in contrast with the previous assignments of McCormack *et al.* [25] and Lefebvre-Brion [29,30].

Sommavilla and Merkt [31] were careful to state, however, that, in principle, perturbations could cause a $^1\Pi_u$ state to look like a $^1\Sigma_u^+$ state. Thus, the absence of Q branches could have several explanations. First, there may be no $^1\Pi_u$ states in this energy region, that is, the states are indeed all $^1\Sigma_u^+$ states. This conclusion appears

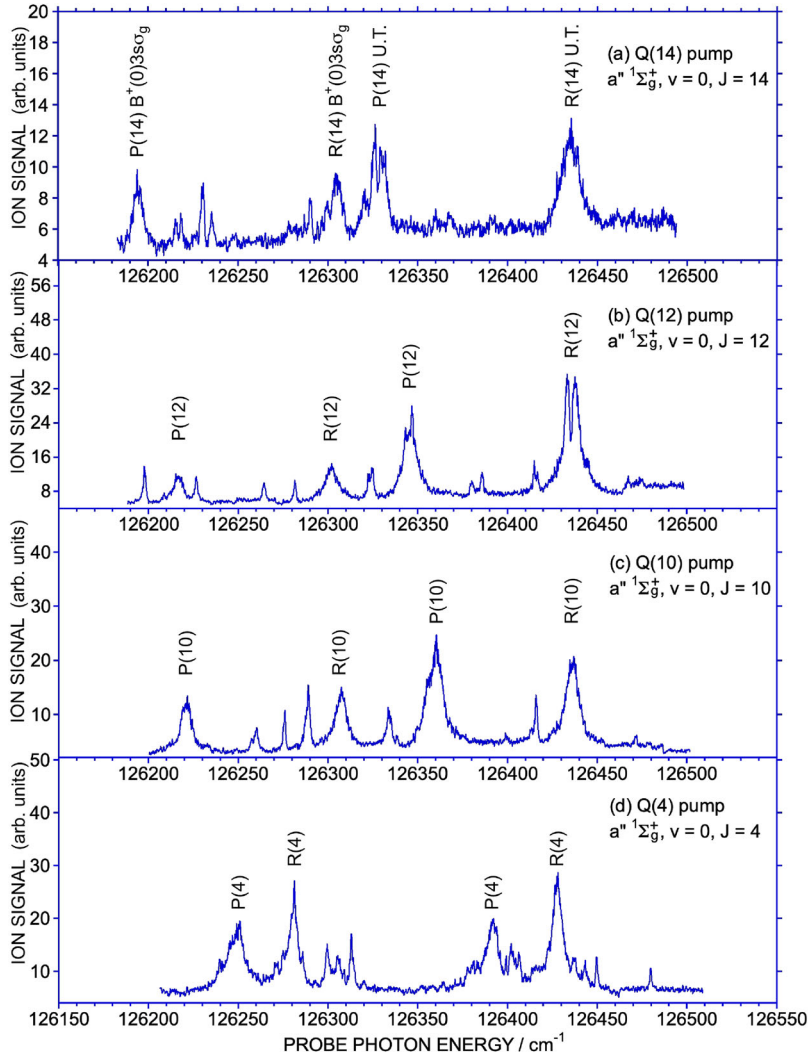

Figure 3. Double-resonance spectra pumping selected rotational levels in the $a''^1\Sigma_g^+, v'' = 0$ state, and probing in the region of Figure 1. The x-axis corresponds to the total transition energy from the relevant rotational level of the ground state, so as to have the same energy axis as Figure 1. 'U.T.' stands for 'upper tower'.

Table 1. Term energies and rotational constants from Figure 4.

Assignment	T_v (cm^{-1})	B_v (cm^{-1})[a]
$B^+(0)3s\sigma_g\,^1\Sigma_u^+$[b]	126269.0	1.89
$b'43$	126325.4	0.87
upper tower	126412.2	1.83
$b'44$	126429.6	0.58
$b'45$	126498.8	0.57

Note: [a] The uncertainty in B_v is estimated to be ~ 0.05 cm^{-1} [b] Assignment according to Ref. [25]

to be most plausible, although some previous work suggests that several $^1\Pi_u$ bands are expected in this region. Furthermore, there are a limited number of $^1\Sigma_u^+$ states to account for all of the observed transitions in this region. Second, as considered by Sommavilla and Merkt [31], the $^1\Pi_u^-$ component of the $^1\Pi_u$ state may be highly perturbed, which could cause the Q-branch transitions accessing it to be unrecognisable as such. If there is a Q branch, the widths of these lines must either be considerably smaller or considerably larger than those for the P and R branches, and the position of the Q branch must be considerably shifted from its expected position. This explanation would require a heterogeneous perturbation by a $^1\Sigma_u^-$ state or other state that only interacts with the $^1\Pi_u^-$ component of the expected state.

As a variation on this second possibility, a third possibility is that the $^1\Pi_u^-$ component is strongly predissociated, thus eliminating the expected rotational structure. Several $^3\Pi_u^-$ states in this energy region are thought to contribute to the dissociative recombination of $N_2^+ + e^-$ [56,57], but predissociation of a $^1\Pi_u$ state by these states is not expected to be selective for the $^1\Pi_u^-$ component relative to $^1\Pi_u^+$. In principle, heterogeneous predissociation by a $^1\Sigma_u^-$ state could produce this selectivity. If

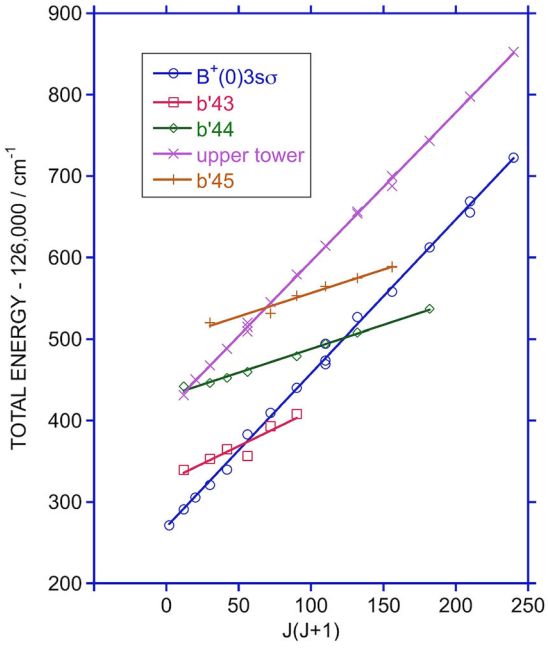

Figure 4. Rotational energy levels as a function of $J(J+1)$. The term energies and rotational constants are given in Table 1.

the predissociation process is selective for the $^1\Pi_u^-$ component of the $^1\Pi_u$ state, the photoionization spectrum would not show any evidence of a Q branch, but the photoabsorption spectrum would still be expected to show a broad absorption feature corresponding to excitation of the strongly predissociated component. It is difficult to determine if there is a significant difference between the jet-cooled photoionization and photoabsorption spectra of Sommavilla and Merkt [31]. However, Shaw *et al.* [27] have performed a detailed analysis of their room-temperature photoionization and photoabsorption cross sections and extracted the wavelength dependent quantum efficiency for ionisation. This efficiency varies between about 0.5 and 0.7 across this region, with minima of $\sim$0.5 at the peaks of the two cathedral bands. Thus, predissociation is clearly an important process for these bands. (Fluorescence is not expected to be important, as the ~ 5 cm^{-1} linewidths of the band responsible for the second tower implies a ps lifetime, while typical fluorescence lifetimes are on the order of ns). Unfortunately, while the extent of predissociation would certainly be sufficient to eliminate the Q-branch transition, the spectra of Shaw *et al.* [27] are not of sufficiently high resolution to determine if there is preferential predissociation for $^1\Pi_u^-$ levels. Thus, the assignment of the upper cathedral tower as a $^1\Pi_u$ state still cannot be ruled out entirely.

Figure 4 shows the rotational term energies from these assignments for the upper states responsible for the two towers and for the $b'43$, $b'44$, and $b'45$ levels, along with linear fits to the data. The rotational term energies, rotational constants, B_v, and vibronic term energies, T_v, are given in Table 1. Differences between the present data and previous determinations are relatively small and primarily due to the different range of rotational levels included in the fits. McCormack and coworkers [25] fit only levels with $J < 10$, and Sommavilla *et al.* [28,31] were constrained to low J levels by their low rotational temperature. For example, a fit to only our lowest five rotational levels of the $B^+(0)3s\sigma_g$ state yields $T_0 = 126,269 \pm 2\text{cm}^{-1}$ and $B_0 = 1.70 \pm 0.05\text{cm}^{-1}$, in excellent agreement with the earlier work. The uncertainties in the data preclude the fitting of higher order rotational constants, e.g. D_v. The $b'45$ level has not been observed previously, but the observed energy and rotational constant are reasonably consistent with those of the $b'43$ and $b'44$ levels.

Figure 4 shows how the $b'43$, $b'44$, and $b'45$ valence states cross the $B^+(0)3s\sigma_g$ and upper tower states over a range of J levels. In particular, the $b'44$ state crosses the upper tower state at low J, exactly the region accessed in the jet-cooled spectra. At these intersections, the rotational energies of both states are affected. In addition, both the intensities and the linewidths of the b' rotational levels appear to increase near these intersections. Indeed, at first glance, the relatively large intensities for transitions to such high vibrational levels of the $b'\ ^1\Sigma_u^+$ state are surprising, but they can be understood by intensity-borrowing from the Rydberg states that do have large intensities. Away from the crossings, the intensities of these transitions diminish substantially.

The probe spectra for a small number of pump transitions show unexpected behaviour for the strong transitions to the upper tower. For example, in Figure 3, the $R(12)$ transition to the upper tower appears to be split. The $R(10)$ transition also shows signs of possible splitting, though it is difficult to tell with the signal-to-noise ratio of the data. Because these unexpected features appear for the strongest transitions, it is possible that they are produced by saturation effects resulting from the excitation of a large fraction of the molecules in the intermediate state. The present double-resonance linewidths for the tower transitions are somewhat larger than previously reported, suggesting that saturation is important. However, the same features are observed for the $R(J-1)$ and $P(J+1)$ transitions, i.e. for different pump transitions and different probe branches, and they are also observed in multiple spectra under different conditions. The most prominent examples of this behaviour occur for the $R(6)$ and $P(8)$ and $R(7)$ and $P(9)$ transitions to the upper tower. As seen in Figure 4, the upper states ($J = 7$ and 8, respectively) occur at just the location that

the $b'45$ state crosses the upper tower, again suggesting that perturbations may be responsible for the unexpected lineshapes.

3.2. Vacuum-ultraviolet Fourier transform spectra from the synchrotron SOLEIL

The local analysis presented above does not provide sufficient information to confirm the assignment, and a more global approach to the spectrum and analysis may be required for a definitive explanation. To this end, Figure 5 shows the high-resolution photoabsorption spectrum of $^{14}N_2$ between 113,000 cm^{-1} and 152,000 cm^{-1} taken with the flowing cell at 77 K and with a resolution of 0.33 cm^{-1}. The full spectrum contains over 700,000 data points and, as seen in Figure 1 and in the next section, many bands show extensive rotationally resolved structure. These data are available in digital form [58], as are the analogous spectra recorded at room temperature in the same cell, and at $\sim$18 K in a supersonic jet. The 77 K spectrum provides a compromise between simplification and preservation of sufficient rotational structure to allow analysis. These data have not yet been exploited and analysed in detail so far, but they will constitute the main input for a comprehensive quantitative analysis, an extension of the type of treatment discussed in Section 2.3.

4. Results: MQDT calculations

The previous MQDT treatment of the rovibronic dipole-allowed $^{14}N_2$ absorption spectrum was limited to a range lower than the $X^+(0)$ level [19]. As previously, the absorption transitions from the ground state are here calculated as transitions between bound states, which means, for instance, that electronic autoionisation of Rydberg states associated with the A^+ core above the IP is disregarded at this point. Also, in this initial exploratory stage, we consider only relative intensities, disregarding the absolute cross section values that can be extracted from the observed data.

Figure 6 shows a partial overview of the VUV FT spectrum, extending from the Rydberg region below the ionisation potential up to the $A^{+2}\Pi_u$ state, recorded at a temperature of 77 K and displayed alongside the MQDT calculations carried out for this temperature with the quantum defect parameters and theoretical framework from Ref. [19]. The observed spectrum is plotted upward whereas the calculated spectrum is plotted downward.

In the region below the ionisation potential where the quantum defects had originally been determined, there is practically a one-to-one correspondence between

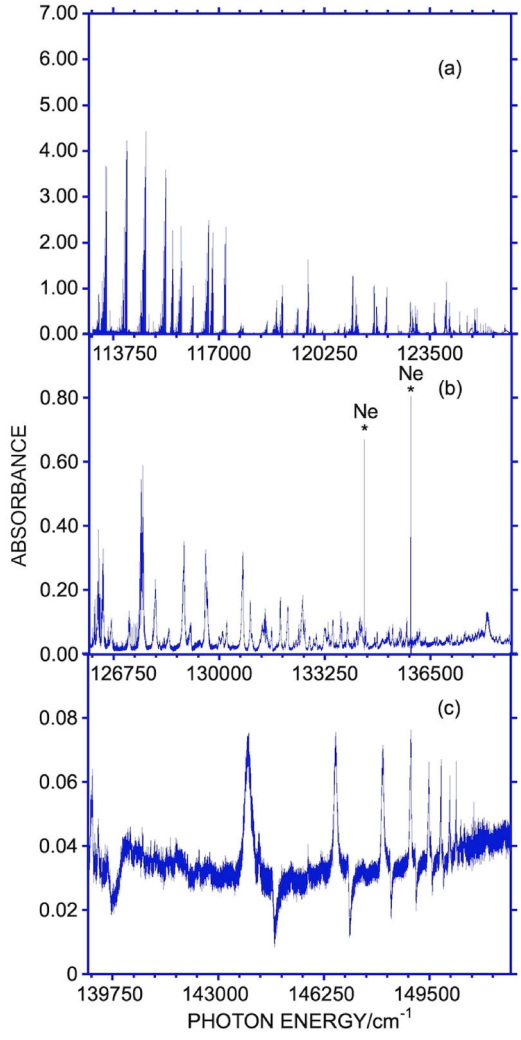

Figure 5. The FT-VUV photoabsorption spectrum of $^{14}N_2$ recorded in this work at 77 K in a flowing cell.

experiment and theory. This is true on the scale of the Figure that does not show the details of the rovibronic structure. As will become apparent below, on a yet enlarged scale the agreement is not everywhere perfect even below the IP. Above the IP, the observed and calculated spectra get gradually out of step and, as the A^+ state is approached, there is only a slight resemblance between the two. Nevertheless it can also be seen that a number of observed major peaks can be identified without problem in the calculated spectrum, while others, such as the cathedral bands, are absent.

For a more detailed discussion, we choose here the vibrational progression of the $A^+(v^+)(4s+3d)\sigma$ (referred to as $A^+(v^+)'3d'\sigma$ in the previous papers [19,20]), which produces a progression of prominent peaks in the absorption spectrum.

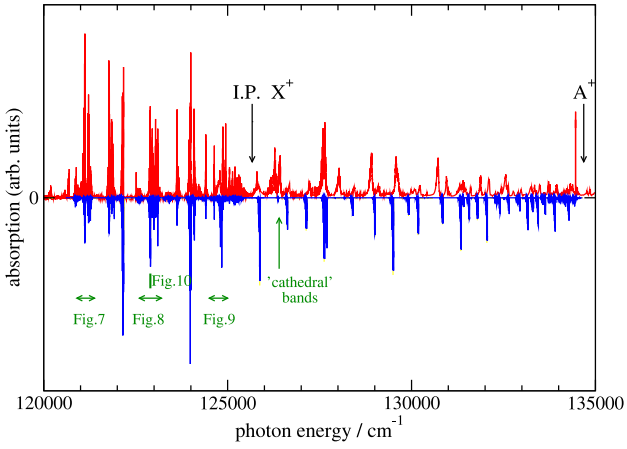

Figure 6. Expanded section of the spectrum of Figure 5. Top: overview of the VUV FT synchrotron dipole absorption spectrum from the $X\ ^1\Sigma_g^+$ ground state of $^{14}N_2$ from below the ionisation potential $X^+\ ^2\Sigma_g^+$ up to the $A^{+2}\Pi_u$ threshold (plotted upward, red online). The gas temperature is 77 K. Bottom: Calculated spectrum for the same region, based on the MQDT parameters taken without change from the previous Ref. [19]. These parameters had been determined based on the rotational analysis of the transitions in the restricted region from 118000 to 125300 cm^{-1} (plotted downward, blue online).

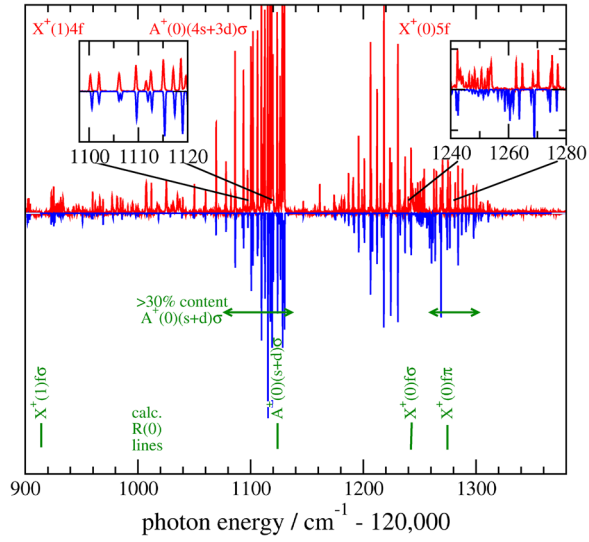

Figure 7. Expanded section of the spectrum (77 K) of Figure 6 in the region of the $A^+(0)(4s+3d)\sigma$, $^1\Pi_u$ core-excited vibronic level. The calculated discrete spectrum has been convoluted with a width corresponding to 0.3 cm^{-1}. The calculated $R(0)$ lines, close to the vibronic band origins, are indicated at the bottom and labelled according to the largest component of the excited state eigenvector (green online). The regions where the $A^+(0)(4s+3d)\sigma$ channel is dominant are indicated by double-headed arrows. The nominal spectroscopic assignments are given at the top. Two insets display enlarged views of selected intervals.

4.1. The $A^+(v^+)(4s+3d)\sigma$ progression

4.1.1. $A^+(0)(4s+3d)\sigma$

On an expanded scale, Figure 7 displays the region from 120,900 to 121,380 cm^{-1}, which had previously been studied in detail in Ref.[19] where the two dominating bands had been assigned to the transition to the $A^+(0)(4s+3d)\sigma$, $^1\Pi_u$ and the $X^+(0)5f\lambda$, $^1\Lambda_u$ ($\lambda = 0-3, \Lambda = 0-3$) components. Overall, the Figure confirms the agreement to within ≈ 1 cm^{-1} between experiment and theory achieved in the earlier Ref. [19]. Note that the core excited vibronic state called $A^+(0)'d'\sigma$ is referred here as $A^+(0)(s+d)\sigma$, indicating the nearly 1:1 mixture of $\ell = 0$ and 2 orbital components. Logically, the companion state $A^+(v^+)'s'\sigma$ will be referred to below as $A^+(v^+)(s-d)\sigma$. Two insets in Figure 7 display the experimental and theoretical spectra on a yet expanded scale. In the case of $A^+(0)(4s+3d)\sigma$ there is a nearly one-to-one correspondence between experiment and theory, whereas in the case of $X^+(0)5f$ the agreement is less good because the calculated $Q^{(f)}$-branch of the (nominal) $5f\phi$ component near 121,260 cm^{-1} is strong, but is not visible in the experimental spectrum. This branch turns up however, in the FT spectra taken at higher pressure (not shown). The calculated eigenvectors indicate (as had been recognised already in Ref. [19]) that $A^+(0)(s+d)\sigma$, $^1\Pi_u$ is strongly mixed with $X^+(0)5f\pi$, $^1\Pi_u$, see Figure 7.

4.1.2. $A^+(1)(4s+3d)\sigma$

Figure 8 (122,600–123,200 cm^{-1}) shows a more complicated situation involving the $A^+(1)(4s+3d)\sigma$, $^1\Pi_u$ vibronic state that here interacts with the $X^+(0)6f$, $X^+(0)7p$ and $X^+(1)4f$ manifolds. The eigenvectors obtained in the MQDT calculations indicate that the $A^+(1)(4s+3d)\sigma$, $^1\Pi_u$ component is strongly manifested in a range spanning 250 cm^{-1}, showing that the multichannel interactions here produce a so-called 'complex' resonance [59]. Nevertheless, the overall appearances of the observed and calculated band structures are in reasonably good agreement, particularly when the highly perturbed nature of numerous Rydberg channels is kept in mind (see the detailed discussion presented in section V.C. of Ref. [19]).

The overall good agreement is confirmed by the insets in the Figure that show the details of the rotational fine structure for two selected portions of the energy range shown in the full Figure. On the other hand, a continuum-like hump appears in the observed spectrum with additional overlapping rotational lines in the region of the $X^+(0)7p\sigma$ component near 122947 cm^{-1}, that have no counterpart in the calculated spectrum. This anomaly was already noted in Ref. [19] and was left unexplained there.

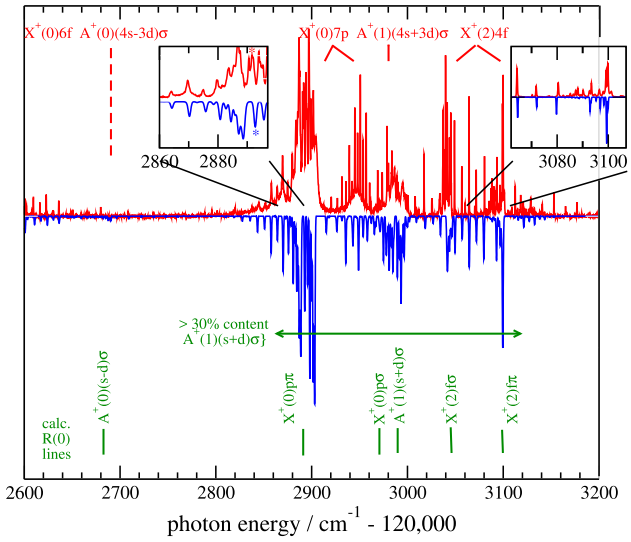

Figure 8. Expanded section of Figure 6 in the region of the $A^+(1)(4s+3d)\sigma$, $^1\Pi_u$ core-excited vibronic level. The calculated discrete spectrum has been convoluted with a width corresponding to 1.0 cm^{-1}. Labels as in Figure 6.

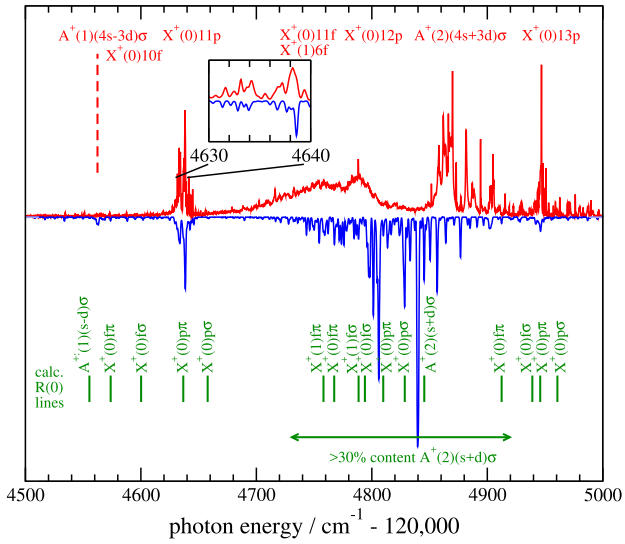

Figure 9. Expanded section of Figure 6 in the region of the $A^+(2)(4s+3d)\sigma$, $^1\Pi_u$ core-excited vibronic level. The calculated discrete spectrum has been convoluted with a width corresponding to 1.0 cm^{-1}. Labels as in Figure 6.

Finally, it must be mentioned that in 2009 Huber and coworkers [20] proposed a partial reanalysis of the cluster of vibronic states represented in Figure 8. This will be discussed in detail in Section 4.2.

4.1.3. $A^+(2)(4s+3d)\sigma$

Figure 9 displays the range 124,500–125,000 cm^{-1}, corresponding to principal quantum numbers $n \approx 11-13$ for Rydberg series converging towards the $X^+(0)$ threshold. The $X^+(0)11p\pi$ and $X^+(0)16p\pi$ Rydberg absorptions have indeed been assigned in Ref. [19], whereas the strong broad feature covering a range of $\sim 150\ cm^{-1}$ around 124,750 cm^{-1} constitutes the first major gap in the otherwise rather complete analysis of Ref. [19].

The theoretical spectrum displayed in the Figure has again been calculated for a temperature of 77 K and is compared with the corresponding VUV FT spectrum. While the spectral resolution of the experimental spectrum nominally is 0.3 cm^{-1}, Figure 9 shows that some spectral lines, and in particular the $X^+(0)11p\pi$ and $X^+(0)13p\pi$ Rydberg band lines, indeed exhibit about this width (see inset), whereas the broad unknown feature appears to consist of far broader rovibronic lines, very probably because of predissociation. For better comparison we have convolved the theoretical spectrum with an *ad hoc* width of 1 cm^{-1}, which is a compromise between the various features appearing in the experimental spectrum.

The present calculations show the following: (i) the strong observed $X^+(0)np\pi$ series of bands is quite well reproduced, although the assumed effective width of the calculation is too large (see the inset where the calculated rotational structure has been convoluted with a width of 0.3 cm^{-1}). (ii) The broad many-line peaks near 124,750 and 124,790 cm^{-1} are, overall, reasonably well reproduced, despite the fact that experimentally the rovibronic structure is largely smeared out, which is not the case with the *ad hoc* width chosen for the plot of the calculated spectrum. (iii) The strong band observed near 124,860 cm^{-1} and extending up to about 124,890 cm^{-1} may be identified in the calculated spectrum by assuming that the calculation positions it about 20 cm^{-1} too low. The assumed effective width here is qualitatively correct.

The positions and intensities of the $R(0)$ transitions indicated at the bottom of Figure 9, show which vibronic Rydberg states are expected to contribute to the spectrum in the region shown according to the present calculation. It is instructive to examine the eigenvectors of the calculated peaks obtained in the MQDT calculation. It turns out that virtually all the calculated levels are predicted to be subject to strong channel coupling, whereby each level contains numerous significant components. The assignments indicated in the Figure correspond for the most part to just the largest components, and serve really only for book keeping purposes. The calculation predicts that, again, a single vibronic level, $A^+(2)(4s+3d)\sigma\ ^1\Pi_u$ dominates the spectrum over as much as 200 cm^{-1}, with all levels containing 30% or more character of the central component. This reveals the presence of another 'complex resonance'. With this in mind, we see that the broad observed feature centred at 124,760 cm^{-1} must be due largely to $X^+(0)$ and $X^+(1)$ f channel components,

whereas the somewhat sharper peak near 124,790 cm^{-1} represents the $X^+(0)$ 12p channels – again reproduced by the calculation only to within $\sim$15 cm^{-1}.

An interesting feature in Figure 9 is the prediction of a weak absorption feature near 124,562 cm^{-1} corresponding to the $A^+(1)(4s-3d)\sigma$, $^1\Pi_u$ vibronic state. The observed spectrum does indeed show a group of weak lines that might represent transitions to this level. In Ref. [19] this weak absorption is not mentioned, but two absorption lines had been attributed to the vibrationless companion, $A^+(0)(4s-3d)\sigma$ $^1\Pi_u$ near 122,600 cm^{-1}, of the feature discussed here. The corresponding energy is marked in Figure 8, but it is not clear whether the predicted weak absorption structure has a counterpart in the observed spectrum. The reassignment of $A^+(0)(4s-3d)\sigma$ $^1\Pi_u$, proposed in Ref. [20], is discussed in the following Section 4.2.

4.2. The 2009 reassignments of Huber et al. [20]

In 2009, Huber and coworkers [20] revisited some of the vibronic assignments made in the earlier 2003 paper [19]. They did this based on new absolute band oscillator strength measurements, as well as on isotope shift measurements between the $^{14}N_2$ and $^{15}N_2$ isomers that had not been used in the earlier analysis of Ref. [19].

In their paper Huber and coworkers state that their new f-value measurements 'update and expand' the 'earlier survey of preliminary data published in 2003' [19]. Further, 'the most radical changes occur near 123,000 cm^{-1}', where 'the photoelectric spectra reveal a shoulder on the high energy side of $X^+(0)7p\pi$ which can be viewed as the head, at 122,907 cm^{-1}, of a red-shaded diffuse band mostly hidden by $X^+(0)7p\pi$'. This shoulder occurs at the sharp drop of the cross section visible in Figure 8 at 122,907 cm^{-1}. Huber and coworkers then assigned this additional band as the transition to the $A^+(1)(4s+3d)\sigma$ $^1\Pi_u$ upper state, thus changing the 2003 assignment where the band at 122,980 ($R(0)$ line at 122,991.26 cm^{-1} [19], called there $A^+(1)3'd'\sigma$, had been associated with this upper state. To complete the assignments in this region these authors attributed the 122,980 cm^{-1} band (that now had become 'free') to the $A^+(0)(4s-3d)\sigma$ vibronic upper state (called there $A^+(0)4's'\sigma$, see Figure 3 of [20]).

Figure 10 illustrates the situation near the $X^+(0)7p\pi$ band head, as it appears in the new VUV FT spectrum. The Figure compares, on a yet expanded scale, the observed and calculated R branch leading to the $X^+(0)7p\pi$ vibronic state. The differences observed – calculated correspond exactly to those of Table II in the 2003 paper [19]. These differences evolve between $R(0)$ and $R(6)$ from -1.1 to $+1.3$ cm^{-1}: clearly, the 2003 global fit placed the position of the vibronic upper state at the correct position, but was unable to reproduce the rotational spacings correctly. The position of the shoulder observed in Ref. [20] is indicated in Figure 10. Visually, the way the shoulder appears in the Figure tends to suggest that it consists of higher members of the $X^+(0)7p\pi$ $R(0)$ branch. In the calculation, the shoulder is inadequately reproduced by the 2003 quantum defect parameters, which predict a band-head at 122,903 cm^{-1}. Note that the VUV FT spectrum shown here has a threefold increased spectral resolution as compared to the spectrum reported in Ref. [20].

This argument appears to lead to the conclusion that the reassignment made in Ref. [20] was not justified. Indeed, it seems unlikely, in view of the strong and well-documented channel interactions coupling the Rydberg states of N_2 built on the X^+ and A^+ cores, that two vibronic origins could come as close as 6 cm^{-1} (see top of the present Figure 10). Considering the quantum defects determined in Ref. [19] we expect a $^1\Pi_u \sim {}^1\Pi_u$ interaction between $X^+7p\pi$ and $A^+(4s+3d)\sigma$ that should be an order of magnitude larger.

In their 2009 paper, Huber and coworkers [20] strengthened their argument in favour of the reassignment further, by considering isotope shifts. They state that 'unambiguous evidence that the $^{14}N_2$ absorption at around 122,888 cm^{-1} is due not to one, but two transitions comes from the spectrum of $^{15}N_2$'. Indeed, they found (see Figure 3 and Ref. [32] of their paper) that the strong band around 122,988 cm^{-1} appears to split into two strong peaks, one of which moves down to 122,839 cm^{-1} indicating the presence of a quantum of vibrational energy in the upper state responsible for the shifted peak. This then points to the presence of the $A^+(1)(4s+3d)\sigma$ $^1\Pi_u$ vibronic state, and appears to confirm the reassignment proposed in Ref. [20]. This shift, down to 122,839 cm^{-1}, is indeed visible also in the present VUV FT spectrum as shown by Figure 11.

By accounting for the known isotope shifts in the rovibrational levels of the X^+ and A^+ core states required in the MQDT rovibronic calculations, but taking over the quantum defects matrices unchanged from [19], we have now calculated the $^{15}N_2$ absorption spectrum shown in the lower part of Figure 11 and compare it with the $^{14}N_2$ spectrum shown in the upper part of the Figure. While the agreement is far from perfect, we see that the MQDT calculation correctly predicts the gross features in both spectra and in particular, qualitatively, the magnitude of the isotope shifts in the various bands. These exhibit a variety of different rotational shapes that are difficult to follow from one isotope to another. It becomes clear at this stage that the usual isotope rules [52] are of no use in highly perturbed situations such as encountered here.

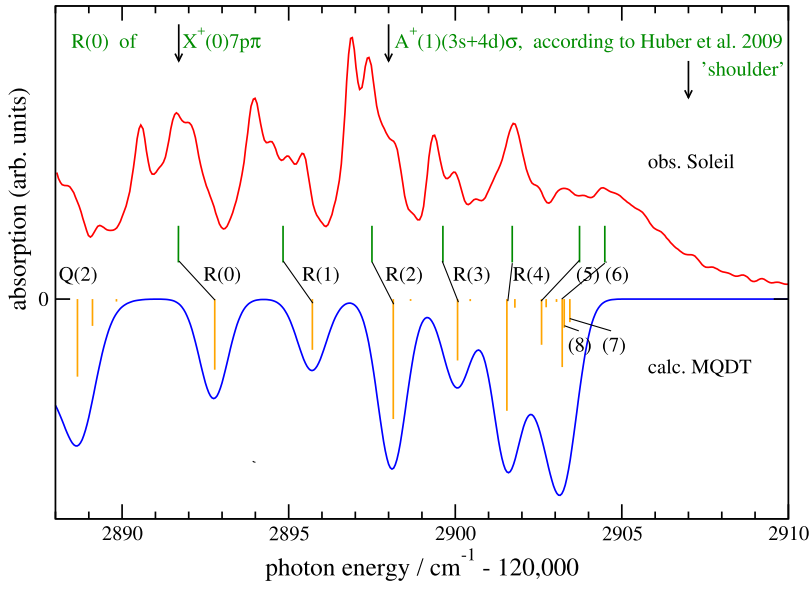

Figure 10. Expanded section of Figure 8 showing the *R* branch of the absorption transition to $X^+(0)7p\pi\,{}^1\Pi_u$ (77 K), as observed by VUV FT spectroscopy (plotted upward) and calculated by MQDT with the 2003 quantum defect parameters [19] (plotted downward). The measured and calculated discrete line positions according to Ref. [19] are indicated in green and in yellow, respectively. The $R(0)$ lines according to Ref. [20] are indicated at the top.

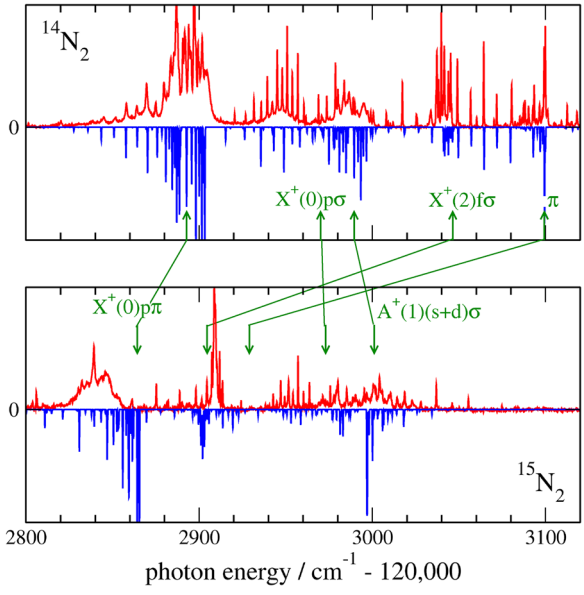

Figure 11. Observed (VUV FT, plotted upward, red online) and calculated (MQDT, plotted downward, blue online) absorption spectra of $^{14}N_2$ (top) and $^{15}N_2$ (bottom) taken at 77 K in the region of 122,900 cm^{-1}. The assignments indicated are based on the eigenvectors of the calculated upper states of the $R(0)$ transitions, indicated by arrows (green online).

Based on this finding we abandon the reassignment proposed in the 2009 paper [20]. The arguments put forward in this older paper were correct as such, but they were limited to a state-to-state analysis of the situation at hand, disregarding the strong channel mixings active within the 'complex' resonance present here. It was thought at the time that the large isotope shift of the $X^+(0)7p\pi$ peak was due to an underlying second quantum state, whereas in fact both these components *co-exist within the same state*, see Figure 8.

To summarise, spectra of different isotopes, such as $^{14}N_2$, $^{14}N^{15}N$ and $^{15}N_2$ of interest here, are expected to provide insight into the vibrational numbering of observed bands [52]. However, the present example of the group of vibronic states interacting with the core-excited $A^+(1)(4s+3d)\sigma$ Rydberg state underlines the fact that these rules may not be helpful in perturbed situations involving states of different vibrational quantum numbers, and can lead to erroneous conclusions. This must also be kept in mind in the discussion of the assignment of the cathedral bands in the following Section 5.

5. Discussion: the assignment of the cathedral bands

We return at this point to our point of departure, the discussion of the cathedral bands. Their definite assignment must await the extended studies proposed here, but a few remarks can already be made.

The large intensity of the bands contributing to the two towers indicates that they almost certainly must be associated with allowed transitions to $A^+(v^+)n\ell\lambda_g$ and $B^+(v^+)n\ell\lambda_g$ Rydberg states. The Franck-Condon factors from the $a''\ {}^1\Sigma_g^+, v=0$ levels to the $X^+(v^+\geq 1)n\ell\lambda_u$ Rydberg states are small, and thus not expected to produce such strong features. Similarly, while transitions to

$^3\Sigma_u^+$, $^3\Pi_u$, and $^1\Sigma_u^-$ Rydberg states and very high vibrational levels of the $b'\ ^1\Sigma_u^+$ valence state have all been discussed in the context of the N_2 spectrum in this region, such transitions are generally observed through intensity borrowing from strong allowed transitions. It is unlikely that any of these nominally forbidden states can produce features with the observed intensities of the two towers on their own.

In agreement with the previous work of Sommavilla *et al.* [28,31] our spectra demonstrate that the state responsible for the higher energy tower manifests as a $^1\Sigma_u^+$ state. Indeed, the experiments to date show that the principal features of both towers of the cathedral have the appearance of $^1\Sigma_u^+$ states. Strong perturbations or selective predissociation of the $^1\Pi_u^-$ component of a $^1\Pi_u$ state could give the appearance of a $^1\Sigma_u^+$ state, but we cannot provide any definitive evidence for this possibility. The isotopic data suggest that the states responsible for both towers have vibrational quantum number $v = 2$, which is not consistent with any of the current assignments of these features, but, as stated above in Section 4.2, vibrational isotope shifts can also be affected by perturbations.

Returning to the schematic energy level diagram of Figure 2, in some cases, transitions to the $A^+(v^+)n\ell\lambda_g$ and $B^+(v^+)n\ell\lambda_g$ Rydberg states have been observed and analysed, while in other cases the transition energies have been estimated from the position of the corresponding $v = 0$ bands and the vibrational energies of the corresponding ion states. The only $^1\Sigma_u^+$ states in this plot correspond to the $A^+(v^+)3d\pi_g$ and $B^+(v^+)3s\sigma_g$ configurations. The expected energy for $B^+(0)3s\sigma_g$ is consistent with its assignment to one of the towers. The $v = 2$ level of the $A^+(v^+)3d\pi_g\ ^1\Sigma_u^+$ progression is predicted to lie closest to the region of interest, but at 127,030 cm^{-1}, the energy is still $\sim$610 cm^{-1} above the observed energy of the higher energy tower. While this assignment would be consistent with the observed vibrational isotope shifts, it seems rather unlikely that the $A^+(2)3d\pi_g\ ^1\Sigma_u^+$ state would be shifted so far from its expected position.

In contrast to the $^1\Sigma_u^+$ states, there are at least two configurations that are predicted to give $^1\Pi_u$ states in the region of the second tower: $A^+(2)(4s - 3d)\sigma_g$ and $A^+(3)(4s + 3d)\sigma_g$ (in our present notation). Both states are expected within 250 cm^{-1} of the observed transitions. Lefebvre-Brion has presented an alternative assignment for a number of the lower energy $A^+(v^+)n\ell\lambda_g$ levels, and in her model, the $A^+(1)(4s + 3d)\sigma_g$ state occurs at an energy consistent with the higher energy tower [29,30]. The assignment to $A^+(2)(4s - 3d)\sigma_g$, which was proposed by McCormack *et al.* [25], is the only one consistent with the observed vibrational isotope shift.

As discussed above, the assignment of the upper tower to a $^1\Pi_u$ state would require a mechanism for the strong, selective predissociation of the $^1\Pi_u^-$ component of this. The most likely state producing such selective predissociation would then be a $^1\Sigma_u^-$ state; a $^3\Sigma_u^-$ state could also provide this selectivity, but the interaction is expected to be considerably weaker. Electronic structure calculations have described two $^1\Sigma_u^-$ states that could possibly account for this predissociation. First, in an early theoretical study, Michels [60] found a repulsive $^1\Sigma_u^-$ state dissociating to $N\ ^2D + N\ ^2D$ that crosses the outer turning points of the $X^+\ ^2\Sigma_g^+$ and $A^+\ ^2\Pi_u$ potentials at $\sim$145,200 cm^{-1}. This energy is somewhat too high to account for predissociation of a $^1\Pi_u$ state near 126,420 cm^{-1}, but it would be interesting to see if this Σ_u^- potential is significantly changed with the higher accuracy methods now available. The second state corresponds to the bound $a'\ ^1\Sigma_u^-$ state, with a term energy of 67,739.290 cm^{-1}. This state also dissociates to $N^2D + N^2D$ at an energy of 117,163 cm^{-1}, and thus provides an open dissociation channel. The shape of this potential is such that its crossing or near-crossing with the potential of the $A^+(2)(4s - 3d)\sigma$ (or other) $^1\Pi_u$ Rydberg state would occur near the inner turning point of the potential. Unfortunately, at this time neither of the potentials is characterised well enough to assess this interaction quantitatively.

It is also interesting to examine the isotope shifts of the cathedral bands. Randazzo *et al.* [35] have previously measured isotopes shifts in photoionization for the cathedral bands for $^{14}N_2$, $^{14}N^{15}N$ and $^{15}N_2$. From the observed shifts, they concluded that the upper state responsible for the higher energy tower has an $A^+(2)$ core, consistent with the assignment of McCormack *et al.* [25] as an $A^+(2)4s\sigma$ Rydberg state. Figure 12 shows portions of the present high-resolution, room-temperature absorption spectra in this region for the three isotopologues. The lower energy tower appears to be breaking up in the $^{15}N_2$ spectrum, and the assignment of the dominant feature is somewhat ambiguous. The observed shifts of the higher energy feature are consistent with those of Randazzo *et al.* [35] and with their $A^+(2)$ assignment. The results are summarised in Table 2, along with predicted shifts for different vibrational levels of the $X^+(v^+)$, $A^+(v^+)$, and $B^+(v^+)$ ions.

Randazzo *et al.* [35] did not discuss the isotope shifts for the lower energy tower, but their spectra are consistent with the present shifts for that feature. The shifts for this tower are similar to those of the higher energy tower for $^{14}N^{15}N$, but are even larger in the $^{15}N_2$ spectrum. This larger shift is more consistent with a Rydberg state with an $X^+(2)$ or $B^+(2)$ ion core. The former is not expected to have the large intensity observed for this feature, and, as discussed next, the lowest energy $B^+(2)n\ell\lambda_g$ Rydberg state is expected to lie at significantly higher energy.

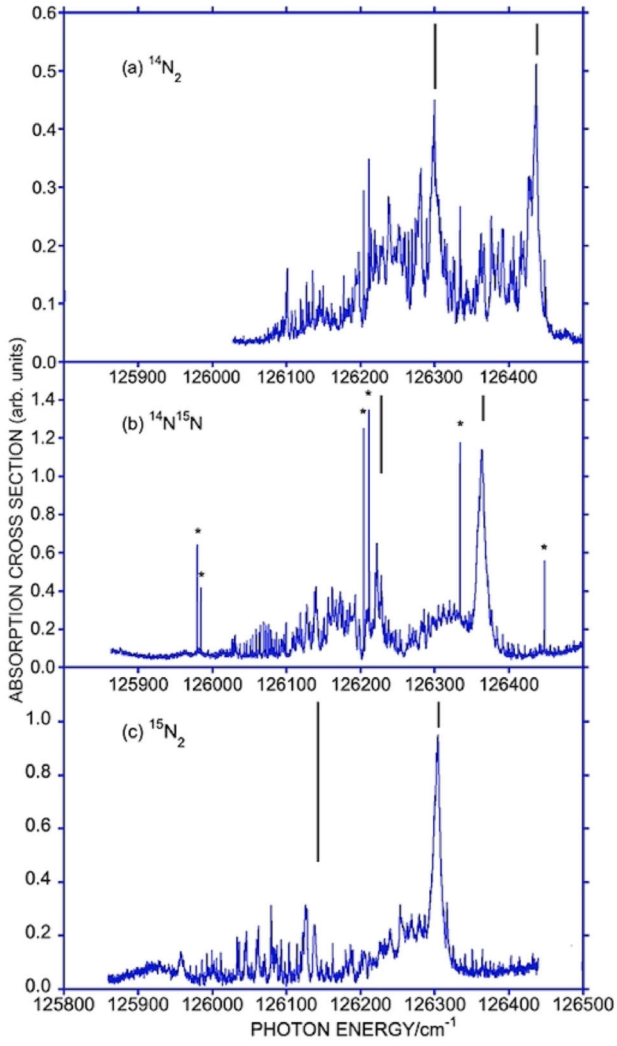

Figure 12. Room temperature FT-VUV photoabsorption spectra between 125,800 cm^{-1} and 126,500 cm^{-1} for: (a) $^{14}N_2$, (b) $^{14}N^{15}N$, and (c) $^{15}N_2$.

Table 2. Isotope shifts for ionisation thresholds from $X\,^1\Sigma_g^+, v'' = 0$.

Vibronic core level	$^{14}N_2 - {}^{14}N^{15}N$ (cm^{-1})	$^{14}N_2 - {}^{15}N_2$ (cm^{-1})
$X^+(0)$ (calc.)	−1.3	−2.6
$X^+(1)$ (calc.)	34.7	70.1
$X^+(2)$ (calc.)	69.2	140.3
$A^+(0)$ (calc.)	−3.8	−7.7
$A^+(1)$ (calc.)	27.2	54.8
$A^+(2)$ (calc.)	57.1	115.3
$A^+(3)$ (calc.)	86.1	173.9
$B^+(0)$ (calc.)	0.4	0.9
$B^+(0)3s\sigma$ (obs.)	71	161
Upper Tower (obs.)	73	132

The allowed Rydberg series converging to the B^+ state of the ion correspond to $B^+(v^+)ns\sigma_g$, $B^+(v^+)nd\sigma_g$, $B^+(v^+)nd\pi_g$, and at higher energy these give rise to the beautiful series of resonances known as the Hopfield series [6]. The $B^+(v^+)4s\sigma_g$, $B^+(v^+)3d\sigma_g$, $B^+(v^+)3d\pi_g$ bands lie near 138900 cm^{-1}, well above the present energy range. From multiple scattering calculations, Kosman and Wallace [15] suggested that the $B^+(0)3s\sigma_g$ state should lie near ∼123,270 cm^{-1}, while the quantum defect for the $B^+(0)ns\sigma_g$ channel determined by Raoult *et al.* [14] puts it at 123,140 cm^{-1}. The assignment of the lower energy tower to $B^+(0)3s\sigma_g$ by McCormack *et al.* [25] is consistent with these estimates. If this state were assigned to $B^+(2)3s\sigma_g$, it would place the $B^+(0)3s\sigma_g$ at ∼121,580 cm^{-1}. Given the existing analysis for that region, the $B^+(2)3s\sigma_g$ assignment for the lower tower appears to be untenable.

Perturbations in the spectra can certainly wreak havoc on the expected isotope shifts, particularly for complex resonances like the cathedral bands that involve interactions among multiple electronic states with different vibrational quantum numbers. We find that for isolated, unperturbed transitions, the isotope shifts are well-behaved and consistent with expected assignments, but for perturbed states and complex resonances, the assignments based on isotope shifts are inconsistent with expectations. In such cases, which include the cathedral region and the complex bands of Figure 11, the isotope shifts are less helpful for aiding or confirming assignments.

Finally, as a new result, Figure 6 shows that the MQDT absorption calculation carried out with the quantum defect functions taken from the 2003 paper [19] does not produce any intense structure in the region of either tower of the cathedral bands. This result points to the tentative conclusion that the cathedral bands would be due to Rydberg structures, presumably a 'complex' resonance, associated with the $B^+\,^2\Sigma_u^+$ core state, not included in the 2003 calculations.

6. Conclusion

A combination of three techniques: double-resonance spectroscopy, high-resolution absorption spectroscopy, and multichannel quantum defect theory (MQDT) has been used to help understand the near-threshold photoionization and photoabsorption spectrum of N_2. The selectivity of the double-resonance process allows an improved characterisation of the rotational structure of the bands responsible for the cathedral features between 126,200 and 126,600 cm^{-1}. The $b'45$ state has been characterised for the first time, and the perturbations between the $b'43$, $b'44$, and $b'45$ valence states and the $A^+(v^+)ns\sigma_g$ and $A^+(v^+)nd\lambda_g$ Rydberg states are better understood. Nevertheless, a definitive and self-consistent set of assignments for the states responsible for the two cathedral towers has not yet been achieved. Although a local assignment of the spectrum appeared to be within reach, the double-resonance spectra could not resolve a

number of the contradictory observations of the previous work. This situation suggests that only a global approach will be able to construct a convincing and comprehensive assignment of the data.

The new photoabsorption data on three isotopologues of N_2 ($^{14}N_2$, $^{14}N^{15}N$, and $^{15}N_2$) span a range of nearly 5 eV with a spectral resolution of 0.3 cm^{-1}, and appear to be ideal input for the MQDT approach, which is global in nature, but at the same time predicts the rotational structure of the individual bands. The detailed analysis of this fine structure, to the extent that it is not washed out by predissociation and autoionisation, will be necessary to arrive at a definite interpretation of the full spectrum. The calculations of $A(v^+)(3d+4s)\sigma\ ^1\Pi_u$ progression presented in Section 4.1 not only demonstrate the capabilities of the MQDT, but also render apparent the limitations of the quantum defect matrices determined back in 2003 [19].

The focus of the discussion here has been mainly on the overall appearance and positions of the peaks observed in the FT-VUV spectrum. Nevertheless, it has already been possible to draw some conclusions from those comparisons. In particular, the important role of 'complex' resonance features has been highlighted.

Acknowledgements

The authors are grateful to the staff at the Synchrotron SOLEIL France for their hospitality and operation of the facility [project numbers 20120023, 20180588, and 20191152]. D.M.P.H. is grateful to the Science and Technology Facilities Council for financial support. S.T.P. was supported by the Gas-Phase Chemical Dynamics Program within the U.S. Department of Energy, Office of Science, Office of Basic Energy Sciences, Division of Chemical Sciences, Geosciences, and Biosciences [contract number DE-AC02-06CH11357].

Author contributions

CRediT: **Ananya Sen:** Investigation; **Nelson de Oliveira:** Investigation; **Ugo Jacovella:** Investigation; **Bérenger Gans:** Investigation; **Séverine Boyé-Péronne:** Investigation; **David M. P. Holland:** Investigation; **Wim Ubachs:** Investigation; **Alan Heays:** Investigation; **Stephen T. Pratt:** Conceptualization; **Christian Jungen:** Conceptualization

Disclosure statement

No potential conflict of interest was reported by the author(s).

ORCID

Ugo Jacovella http://orcid.org/0000-0003-2152-261X
Wim Ubachs https://orcid.org/0000-0001-7840-3756

Data availability statement

The data that support the findings of this article are openly available [58].

References

[1] H. Lefebvre-Brion and R.W. Field, *The Spectra and Dynamics of Diatomic Molecules* (Elsevier, Boston, 2004).
[2] M. Quack and F. Merkt, *Handbook of High-Resolution Spectroscopy*, 3 vols. (Wiley, East Sussex, UK, 2011).
[3] M. Ogawa and Y. Tanaka, Can. J. Phys. **40**, 1593–1607 (1962). doi:10.1139/p62-165
[4] M. Ogawa, Can. J. Phys. **42**, 1087–1096 (1964). doi:10.1139/p64-102
[5] K. Yoshino, M. Ogawa and Y. Tanaka, J. Mol. Spectrosc. **61**, 403–411 (1976). doi:10.1016/0022-2852(76)90331-3
[6] A. Lofthus and P.H. Krupenie, J. Phys. Chem. Ref. Data **6**, 113–307 (1977). doi:10.1063/1.555546
[7] K. Dressler, Can. J. Phys. **47**, 546–562 (1969). doi:10.1139/p69-072
[8] H. Lefebvre-Brion, Can. J. Phys. **47**, 541–545 (1969). doi:10.1139/p69-071
[9] P.K. Carroll and P. Collins, Can. J. Phys. **47**, 563–589 (1969). doi:10.1139/p69-073
[10] D. Stahel, M. Leoni and K. Dressler, J. Chem. Phys. **79**, 2541–2558 (1983). doi:10.1063/1.446166
[11] W. Ubachs, I. Velchev and A. de Lange, J. Chem. Phys. **112**, 5611–5616 (2000). doi:10.1063/1.481145
[12] A. Heays, R. Visser, R. Gredel, W. Ubachs, B.R. Lewis, S.T. Gibson and E.F. van Dishoeck, Astron. Astrophys. **562**, A61 (2014). doi:10.1051/0004-6361/201322832
[13] R.R. Lucchese, G. Raseev and V. McKoy, Phys. Rev. A **25**, 2572–2587 (1982). doi:10.1103/PhysRevA.25.2572
[14] M. Raoult, H. Le Rouzo, G. Raseev and H. Lefebvre-Brion, J. Phys. B **16**, 4601–4617 (1983). doi:10.1088/0022-3700/16/24/016
[15] W.M. Kosman and S. Wallace, J. Chem. Phys. **82**, 1385–1399 (1985). doi:10.1063/1.448461
[16] B. Basden and R.R. Lucchese, Phys. Rev. A **37**, 89–97 (1988). doi:10.1103/PhysRevA.37.89
[17] K.P. Huber and Ch. Jungen, J. Chem. Phys. **92**, 850–861 (1990). doi:10.1063/1.458589
[18] K.P. Huber, Ch. Jungen, K. Yoshino, K. Ito and G. Stark, J. Chem. Phys. **100**, 7957–7972 (1994). doi:10.1063/1.466841
[19] Ch. Jungen, K.P. Huber, M. Jungen and G. Stark, J. Chem. Phys. **118**, 4517–4538 (2003). doi:10.1063/1.1542877
[20] K.P. Huber, M.-N. Chan, G. Stark, K. Ito and T. Matsui, J. Chem. Phys. **131**,084301(2009). doi:10.1063/1.3211309
[21] P.M. Dehmer, P.J. Miller and W.A. Chupka, J. Chem. Phys. **80**, 1030–1038 (1984). doi:10.1063/1.446829
[22] S.H. Southworth, A.C. Parr, J.E. Hardis and J.L. Dehmer, Phys. Rev. A **33**, 1020–1023 (1986). doi:10.1103/PhysRevA.33.1020
[23] M. Zubek, G.C. King and P.M. Rutter, J. Phys. B **21**, 3585–3594 (1988). doi:10.1088/0953-4075/21/21/014
[24] J.B. West, M.A. Hayes, A.C. Parr, J.E. Hardis, S.H. Southworth, T.A. Ferrett, J.L. Dehmer, X.M. Hu and G.V. Marr, Phys. Scr. **41**, 487–489 (1990). doi:10.1088/0031-8949/41/4/024

[25] E.F. McCormack, S.T. Pratt, J.L. Dehmer and P.M. Dehmer, Phys. Rev. A **42**, 5445–5451 (1990). doi:10.1103/PhysRevA.42.5445
[26] E.F. McCormack, S.T. Pratt, J.L. Dehmer and P.M. Dehmer, Phys. Rev. A **44**, 3007–3015 (1991). doi:10.1103/PhysRevA.44.3007
[27] D.A. Shaw, D.M.P. Holland, M.A. MacDonald, A. Hopkirk, M.A. Hayes and S.M. McSweeney, Chem. Phys. **166**, 379–391 (1992). doi:10.1016/0301-0104(92)80097-F
[28] M. Sommavilla, U. Hollenstein, G.M. Greetham and F. Merkt, J. Phys. B **35**, 3901–3921 (2002). doi:10.1088/0953-4075/35/18/309
[29] H. Lefebvre-Brion, J. Chem. Phys. **122**,144315(2005). doi:10.1063/1.1876232
[30] H. Lefebvre-Brion, J. Electron Spectrosc. Rel. Phenom **144-147**, 109–111 (2005). doi:10.1016/j.elspec.2005.01.002
[31] M. Sommavilla and F. Merkt, J. Electron Spectrosc. Rel. Phenom. **151**, 31–33 (2006). doi:10.1016/j.elspec.2005.09.009
[32] D.M.P. Holland and D.A. Shaw, J. Electron Spectrosc. Relat. Phenom. **184**, 144–148 (2011). doi:10.1016/j.elspec.2010.12.006
[33] P. O'Keeffe, P. Bolognesi, A. Moise, R. Richter, Y. Ovcharenko and L. Avaldi, J. Chem. Phys. **136**,104307 (2012). doi:10.1063/1.3692687
[34] D.M.P. Holland, E.A. Seddon, S. Daly, C. Alcaraz, C. Romanzin, L. Nahon and G.A. Garcia, J. Phys. B **46**,095102(2013). doi:10.1088/0953-4075/46/9/095102
[35] J.B. Randazzo, P. Croteau, O. Kostko, M. Ahmed and K.A. Boering, J. Chem. Phys. **140**,194303(2014). doi:10.1063/1.4873717
[36] A.M. Chartrand, E.F. McCormack, U. Jacovella, D.M.P. Holland, B. Gans, X.-F. Tang, G.A. Garcia, L. Nahon and S.T. Pratt, J. Chem. Phys. **147**,224303(2017). doi:10.1063/1.5004538
[37] K. Huber, G. Stark and K. Ito, J. Chem. Phys. **98**, 4471–4477 (1993). doi:10.1063/1.465006
[38] M.O. Vieitez, T.I. Ivanov, W. Ubachs, B.R. Lewis and C.A. de Lange, J. Mol. Liq. **141**, 110–117 (2008). doi:10.1016/j.molliq.2008.01.014
[39] M.O. Vieitez, T.I. Ivanov, J.P. Sprengers, C.A. de Lange, W. Ubachs, B.R. Lewis and G. Stark, Mol. Phys. **105**, 1543–1557 (2007). doi:10.1080/00268970701291750
[40] B.R. Lewis, K.G.H. Baldwin, A.N. Heays, S.T. Gibson, J.P. Sprengers, W. Ubachs and M. Fujitake, J. Chem. Phys. **129**,204303(2008). doi:10.1063/1.3023034
[41] J.P. Sprengers, E. Reinhold, W. Ubachs, K.G.H. Baldwin and B.R. Lewis, J. Chem. Phys. **123**,144315(2005). doi:10.1063/1.2062189
[42] R. Seiler, U. Hollenstein, G.M. Greetham and F. Merkt, Chem. Phys. Lett. **346**, 201–208 (2001). doi:10.1016/S0009-2614(01)00928-9
[43] P. Wang, S. Gong, Y. Li and Y. Mo, J. Chem. Phys. **160**,014304(2024). doi:10.1063/5.0187003
[44] N. de Oliveira, D. Joyeux, D. Phalippou, J.C. Rodier, F. Polack, M. Vervloet and L. Nahon, Rev. Sci. Instrum. **80**,043101(2009). doi:10.1063/1.3111452
[45] N. de Oliveira, M. Roudjane, D. Joyeux, D. Phalippou, J.C. Rodier and L. Nahon, Nat. Photonics **5**, 149–153 (2011). doi:10.1038/nphoton.2010.314
[46] N. de Oliviera, D. Joyeux, M. Roudjane, J.-F. Gil, B. Pilette, L. Archer, K. Ito and L. Nahon, J. Synchrotron Rad. **23**, 887–900 (2016). doi:10.1107/S1600577516006135
[47] F. Aguirre and S.T. Pratt, J. Chem. Phys. **118**, 1175–1183 (2003). doi:10.1063/1.1530582
[48] H. Xu, U. Jacovella, B. Ruscic, S.T. Pratt and R.R. Lucchese, J. Chem. Phys. **136**,154303(2012). doi:10.1063/1.3701762
[49] K.R. Lykke and B.D. Kay, J. Chem. Phys. **95**, 2252–2258 (1991). doi:10.1063/1.460981
[50] M.J.J. Vrakking, A.S. Bracker and Y.T. Lee, J. Chem. Phys. **96**, 7195–7196 (1992). doi:10.1063/1.462528
[51] E.J. Salumbides, A. Khramov and W. Ubachs, J. Phys. Chem. A **113**, 2383–2386 (2009). doi:10.1021/jp808698u
[52] G. Herzberg, *Spectra of Diatomic Molecules* (Van Nostrand Reinhold, New York, 1950).
[53] U. Fano, Phys. Rev. A **2**, 353–365 (1970). doi:10.1103/PhysRevA.2.353
[54] Ch. Jungen and O. Atabek, J. Chem. Phys. **66**, 5584–5609 (1977). doi:10.1063/1.433881
[55] Ch. Jungen and G. Raseev, Phys. Rev. A **57**, 2407–2419 (1998). doi:10.1103/PhysRevA.57.2407
[56] S.L. Guberman, J. Chem. Phys. **139**,124318(2013). doi:10.1063/1.4821595
[57] D.A. Little and J. Tennyson, J. Phys. B: At. Mol. Opt. Phys. **46**,145102(2013). doi:10.1088/0953-4075/46/14/145102
[58] The digital data are available from the authors, and will be placed in the Mainz spectral database (http://www.uv-vis-spectral-atlasmainz.org/uvvis/).
[59] Ch. Jungen and M. Raoult, Farad. Disc. Roy. Soc. Chem. **71**, 253–271 (1981). doi:10.1039/dc9817100253
[60] H.H. Michels, Adv. Chem. Phys. **45**, 225–340 (1981). doi:10.1002/SERIES2007